Radiation effects on the structure and alteration behavior of a SiO_2 -Al_2 O_3 -B_2 O_3 -Na_2 O glass

Amreen Jan, Jean-marc Delaye, Huseyin Kaya, Seong Kim, Anamul Haq Mir, Thibault Charpentier, Frédéric Angeli, Stephane Gin

Received: 28 March 2022 | Revised: 25 August 2022 | Accepted: 29 September 2022

DOI: 10.1111/ijag.16618

INTERNATIONAL JOURNAL OF Applied Glass SCIENCE

SPECIAL ISSUE ARTICLE

Radiation effects on the structure and alteration behavior of an SiO_2–Al_2O_3–B_2O_3–Na_2O glass

Amreen Jan[1] | **Jean-Marc Delaye**[1] | **Huseyin Kaya**[2] | **Seong H. Kim**[2,3,4] | **Anamul Haq Mir**[5] | **Thibault Charpentier**[6] | **Frédéric Angeli**[1] | **Stephane Gin**[1]

[1]CEA, DES, ISEC, DE2D, University of Montpellier, Bagnols-sur-Cèze, France

[2]Department of Materials Science and Engineering, The Pennsylvania State University, University Park, Pennsylvania, USA

[3]Department of Chemical Engineering, The Pennsylvania State University, University Park, Pennsylvania, USA

[4]Materials Research Institute, The Pennsylvania State University, University Park, Pennsylvania, USA

[5]School of Computing and Engineering, Electron Microscopy and Materials Analysis, University Huddersfield, Huddersfield, UK

[6]CEA, CNRS, NIMBE, Université Paris Saclay, Gif-Sur-Yvette, France

Correspondence
Jean-Marc Delaye, CEA, DES, ISEC, DE2D, University of Montpellier, Marcoule, Bagnols-sur-Cèze F-30207, France.
Email: jean-marc.delaye@cea.fr

Funding information
Center for Performance and Design of Nuclear Waste Forms and Containers; Energy Frontier Research Center; U.S. Department of Energy, Office of Science, Basic Energy Sciences, Grant/Award Number: DE-SC0016584; Engineering and Physical Sciences Research Council, Grant/Award Number: EP/ T012811/1

Abstract

As borosilicate glasses are used in many countries to immobilize fission products and minor actinides after spent fuel reprocessing before storage in a deep geological repository, assessing that their chemical durability is of paramount importance. Here, pristine and preirradiated (952 MeV, 136Xe) SiO_2–B_2O_3–Al_2O_3–Na_2O glasses with the same molar ratios as in the French SON68 and ISG glasses have been subjected to aqueous corrosion in deionized water and in silica-saturated solution to measure the initial and longer term alteration rates. Pristine and preirradiated glasses corrode following the same mechanisms, but the preirradiation has a strong impact on the initial dissolution rate (increase by a factor of 5.6), and on the alteration layer depth in silica-saturated conditions (by two- to threefolds). The later result is related to the formation of a more porous, less passivating gel on the preirradiated glass specimen. Using both experimental spectroscopies (NMR, IR, and SFG) and classical molecular dynamics, the radiation effects on the glass structure and water diffusion have been assessed. After preirradiation, the density and the polymerization degree of the glass decrease, whereas the topological disorder increases. In consequence, water diffusion accelerates. These observations allow to correlate the radiation impact on the alteration behavior to the structural changes.

KEYWORDS
alteration , borosilicate, irradiation, molecular modeling, nuclear magnetic resonance, IR spectroscopy

1 | INTRODUCTION

In several countries, borosilicate glasses are proposed to be used to immobilize fission products and minor actinides after spent fuel reprocessing.[1–3] As it is planned to store these glassy matrices in a deep geological disposal, it is important to understand the alteration mechanisms to assess their long-term behavior. Understanding glass alteration by water is a complex problem, and no definitive answer has been provided up to now despite a very rich literature.[4–6] Several models have been proposed. A first model[7,8] postulates that the glass dissolves congruently in a thin film of interfacial water followed by the precipitation of sparingly soluble species responsible for the alteration layer formation at the glass surface. This model is currently successfully applied for minerals.[9] Another model[10,11] postulates that the structure of the first gel formed after preferential leaching of the weakly bonded elements retains the glass structure and then matures to lower its internal energy. In this model, the gel is formed by an incomplete hydrolysis of sparingly soluble glass cations (Si, Al, Zr) followed by local condensation.

In fact, depending on the glass composition, the alteration behavior changes. In a glass containing only SiO_2, B_2O_3, and Na_2O, it has been shown, using solutions enriched with ^{29}Si and ^{18}O, that the alteration layer is formed after complete dissolution followed by the precipitation of the less soluble elements.[12] This conclusion has been drawn because the alteration layer is enriched both in ^{29}Si and ^{18}O and also silica nanoparticles precipitated on the top of the glass surface (TEM observations).[13] When Al_2O_3 is added to this glass, the behavior changes. Although the same solution enriched with ^{29}Si and ^{18}O was used, the alteration layer is only enriched with ^{18}O but not with ^{29}Si. From this observation, it can be concluded that no complete glass hydrolysis occurred, and only a partial hydrolysis of Si–O–M (M = Si, B, Al) takes place accompanied by local condensation. The modification of the behavior upon Al_2O_3 addition has been explained recently by investigating the Al impact on the bond hydrolysis energies.[14,15]

The objective of this paper is to study whether the mechanism of gel formation previously described is impacted by the irradiation of the glass prior to its exposure to aqueous environment. To address this question, we work with an SiO_2–B_2O_3–Al_2O_3–Na_2O glass, called CJ2, corresponding to a simplified nuclear glass with the same molar ratios as in the ISG[16] and French SON68 nuclear glasses.[17] This glass has already been used in previous studies.[12,18]

CJ2 glass has been irradiated by heavy ions (952 MeV ^{136}Xe). This kind of irradiation is able to reproduce the internal radiation effects induced by the minor actinides.[19,20] The glass structure and properties are modified when the deposited nuclear energy increases until a saturation threshold equals roughly 60 MGy. The density decreases by a few percent. The average boron coordination decreases; that is, BO_4 local entities are converted into BO_3 entities.[21] In parallel, the nonbridging oxygen (NBO) concentration increases because of the release of Na ions initially used to compensate the BO_4 entities. These structural modifications could affect the water diffusion inside the glass. It has also been observed that the glass transition temperature increases after irradiation, while an energy of the order of 105 J g^{-1} is stored.[22] The fracture toughness increases and the hardness decreases until a saturation plateau corresponds to the same irradiation threshold energy.[23,24]

Unlike crystals,[25] water diffusion in glass is a preponderant mechanism during the different alteration stages.[5,6,26] When a glass is in contact with water, interdiffusion between the aqueous species and the alkaline ions near NBO (glass modifiers) readily takes place followed by the hydrolysis of the reticulated network. During this stage, called stage I, the glass dissolves congruently. For a given set of temperature and pH, the alteration rate during stage I is maximum and corresponds to the initial (or forward) alteration rate. After this, the solution begins to saturate in Si, and a protective layer progressively forms at the glass–solution interface inducing the decrease of the dissolution rate. But the B and Na ions continue to be released by hydrolysis and ion-exchange mechanisms with the aqueous species. This stage is called stage II. The alteration rate during stage II corresponds to the residual alteration rate. One way to bypass stage I is to perform alteration experiment with a solution initially saturated with amorphous silica.[11,27,28]

In this study, experiments on pristine and preirradiated specimens have been conducted both in deionized water (DIW) and in a solution enriched with Si to investigate the initial and residual alteration regimes. It will be shown that the pristine and preirradiated glasses still undergo the same corrosion mechanisms despite significant difference in the rates.

In order to try to better understand experimental results, classical molecular dynamics calculations have been performed using interatomic potentials that are able to reproduce hydrated glasses.[14,29,30] The objective here is to prepare both pristine and pseudo-irradiated glasses (in fact, fast quenched glasses that present equivalent structural modifications as irradiated glasses) to investigate the water diffusion change after irradiation. We have seen that water diffusion is significantly accelerated in the pseudo-irradiated structure compared to the pristine one, and this process can be put forward to explain some of the experimental results.

TABLE 1 Heavy ion beam parameters

Ion parameter	Value
Ion	^{136}Xe
Energy	~952 MeV (7 MeV u^{-1})
Fluence	7.5×10^{12} ions cm^{-2}
Range	~64 μm
Dose	11×10^{20} keV cm^{-3} (~73 MGy)
Energy loss by electronic ionizations (S_e)	18 keV × nm^{-1}
Energy loss by nuclear collisions (S_n)	.6 keV × nm^{-1}

Note: Range and energy losses were determined using SRIM software.

This paper is organized as follows. The methodological part, experiments, and simulations are presented in Section 2. The results are presented in Section 3 by separating the structural effects due to irradiation, the impact of irradiation on the initial and residual alteration rates, and finally, the radiation impact on water diffusion simulated by classical molecular dynamics. The results are then discussed and compared to literature.

2 | METHODOLOGY

2.1 | Glass preparation

A glass called CJ2 ($64.9SiO_2$, $17.3B_2O_3$, $13.6Na_2O$, $4.1Al_2O_3$ in mol%) was prepared with analytical grade carbonate and oxide powders and melted twice at 1500 and 1450°C, respectively. After the second batch, the glasses were annealed for 3 h at T_g + 20 K. Further, monoliths were prepared by cutting and polishing at various grades up to a diamond suspension of .05 μm, leading to the surface roughness of the order of a few nm. Before use, monoliths were cleaned in acetone and alcohol.

Pristine and irradiated CJ2 glass powders of grain size 6–8 μm were prepared to carry out NMR spectroscopy.

2.2 | Heavy ion irradiation

CJ2 glass monoliths were cleaned with acetone and ethanol and then pasted on aluminum sample holders using carbon tape. Both the polished sides were irradiated at room temperature and at normal incidence with ^{136}Xe ions at the beamline SME at GANIL facility in Caen, France. See Table 1 for the specifications of the ion beam.

The use of this swift heavy ion beam is justified because of the following:

1. The range of ^{136}Xe with an energy of 952 MeV in borosilicate glass was calculated using SRIM software,[31] to be ~60 μm. Hence, the depth of irradiation damage is higher than the alteration depth. This ensures that the effect of irradiation damage on glass dissolution will be studied in the damaged zone. In another paper in preparation, Raman spectroscopy has been used to estimate the penetration depth of the projectiles. According to the R band change versus the depth, it can be deduced that the CJ2 glass is homogeneously irradiated at least over 50 μm, confirming the order of magnitude of the SRIM calculation.
2. Even though swift heavy ion loses energy by electronic collisions, it has been concluded by Mir et al.[32,33] (mono and sequential irradiations) that electronic damages above ion track threshold closely resemble the damages caused by nuclear collision.

The 6–8 μm powder has been irradiated with ^{136}Xe ion beam with parameters exactly the same as for the glass monoliths.

2.3 | Experimental conditions

2.3.1 | Initial dissolution rate experiment

The initial alteration rate experiment was conducted in perfluoroalkoxy (PFA) vessel containing 500 ml DIW heated to 90 ± 1°C, the $pH^{90°C}$ was adjusted to 9 ± .1 with a .1 mol L^{-1} LiOH solution. Glass monolith dimensions were measured with a caliper, and monolith was carefully cleaned with ethanol and put inside the Teflon basket. This basket was then suspended inside the solution vessel using a Teflon tape. To ensure the homogeneity of the solution, a magnetic stirring system was used. The solution was continuously stirred with a magnetic bar. In this configuration, the Reynolds number, a dimensionless number indicating the flow pattern, was estimated to be larger than 2000, a value characteristic of a turbulent flow at the glass surface. The whole experiment was conducted in an oven that was maintained at 90°C. Five milliliters of solution sample was taken with a syringe every hour for about 12 h. The pH and temperature were measured at regular intervals. Solution samples were analyzed by spectrophotometry.

2.3.2 | Passivating gel formation

Starting solution (Table 2) was prepared by diluting $^{29}SiO_2am$ ("am" stands for amorphous) solution with ^{18}O-enriched water such that the final concentration of Si was 339 mg L^{-1}. The $pH^{90°C}$ (adjusted with LiOH) of the onset

TABLE 2 Starting Si-saturated solutions for the short-term test

Starting solution	
C_i(Si) (mg L^{-1})	339.3
$^{29}Si/^{28}Si$	147 ± 9
$^{18}O/^{16}O$	.453

TABLE 3 Glass coupons and solution data at the starting time of the experiments. NIR, IR_1, and IR_2 represent the nonirradiated and the two irradiated glass coupons

Sample	Initial volume (ml)	S/V (cm^{-1})
CJ2_NIR	1.049	1.204
CJ2_IR_1	1.264	1.083
CJ2_IR_2	1.559	.814

solution was 9.0 ± .1. Note that the onset solution was saturated with amorphous silica in order to bypass the transient regime between stage I and stage II and favor the formation of a passivating layer.[27,34,35]

Three glass coupons (one nonirradiated and two irradiated) were altered in ~1.5 ml (may vary) each of starting solution for 33 days, in 7 ml PFA vessel enclosed in a 50 ml vessel containing DIW to ensure the solution does not evaporate. The alteration conditions are given in Table 3.

On the 33rd day, three coupons were removed from the solution and immediately rinsed with 97.1% ^{18}O-enriched water (to avoid interference of the isotopic enrichment of altered layer with atmosphere or DIW) to avoid the precipitation on the glass. One of the irradiated–altered coupons (CJ2_IR_2) was removed from the solution and then immersed for 1 day at room temperature in an isotopically natural water doped with methylene blue and bromothymol blue, two molecules of 1 nm hydrodynamic diameter. Their behavior in the alteration layer is expected to reveal the existence of channels bigger than 1 nm and connected to the bulk solution. These coupons were then analyzed using time-of-flight secondary-ion-mass-spectrometry (ToF-SIMS). Following the ToF-SIMS analysis, an irradiated–altered and a nonirradiated-altered coupon were characterized by SEM and TEM.

The solution used for the 33-day experiment was acidified with 2 ml of 1 N HNO_3 for analysis by inductively coupled plasma–optical emission spectrometry (ICP-OES) and inductively coupled plasma tandem mass spectrometry.

Concentrations of the elements were determined by ICP-OES and/or spectrophotometry. After correcting the concentrations with the respective factor of dilution, the normalized mass losses (NL_i) in g m^{-2} are calculated using the following equation:

$$NL_i = 10^{-2}\frac{C_i}{\left(\frac{S}{V}\right)X_i}$$

where C_i is the concentration in mg L^{-1} of element i in the solution, S/V is the glass surface area to solution volume ratio (cm^{-1}), and X_i is the mass fraction of the element in the glass.

From NL_i, equivalent thickness (ET_i) in μm of the element dissolved from the glass of density ρ_g is given by

$$ET_i = \frac{NL_i}{\rho_g}$$

The initial (r_0)and residual (r_r) rate of glass alteration in g m^{-2} d^{-1} can then be calculated by following the NL_i over time:

$$r(i,t) = \frac{dNL_i(t)}{dt}$$

The initial slope corresponds to r_0 and the final slope to r_r.

2.4 | Solid-state characterization

2.4.1 | NMR

The speciation of boron, aluminum, sodium, and silicon in the pristine and the irradiated glasses were studied by MAS NMR spectroscopy. Data were collected on a Bruker Avance II 500WB Bruker spectrometer operating at a magnetic field of 11.72 T. A Bruker CPMAS 4 mm probe was used at a spinning frequency of 12.5 kHz. For boron-11, aluminum-27, and sodium-23, MAS NMR spectra were acquired using a short single pulse (1 μs) for the homogeneous excitation of the resonances (i.e., for providing quantitative spectra) and a recycle delay ranging from 1 s (^{23}Na, ^{27}Al) to 2 s (^{11}B). In addition, two-dimensional multiple-quantum (MQMAS) spectra were acquired; these experiments provide spectra with a higher resolution (free of quadrupolar second-order broadening that affect the MAS spectra). The MQMAS experiments we performed are described in detail in the studies of Angeli et al.[36] For silicon-29, spectra were acquired using a presaturation delay (about twenty 90° pulses to saturate the signal) followed by a recovery delay of 20 s. For a longer delay (200 s), no change in lineshape was observed.

NMR shifts are reported using external reference samples of aqueous 1 M boric acid (^{11}B, 19.6 ppm), 1 M NaCl (^{23}Na, 0 ppm), and 1 M $Al(NO_3)_3$ (^{27}Al, 0 ppm) of

solid tetrakis(trimethylsilyl)silane (−9.9 ppm for the peak highest intensity, relative to TMS).

Data were processed and fitted using an in-house program (written by T. Charpentier), as described in the studies of Angeli et al.[36]

2.4.2 | ToF-SIMS

ToF-SIMS analyses were performed by TESCAN Analytics (France) with an IONTOF GmbH© TOF 5 spectrometer. Depth profiling was operated in sputtering mode with two primary beams Bi_3^{2+} 25 keV .05 pA and Cs^+ 2 keV 160 nA to record negative ions. The abraded area and the analyzed area were 200 × 200 and 50 × 50 μm^2, respectively. After each cycle of abrasion and analysis, the surface charge was neutralized with a low-energy electron beam (<20 eV). At the end, the crater depth was measured with a 3D profilometer. For more details about the application of the ToF-SIMS technique to glass alteration, see Gin et al.[37]

2.4.3 | TEM specimen preparation and analysis

Leached specimens were attached to a SEM aluminum stub using silver epoxy and then sputter coated with Cr (100–250 nm thick). The FIB/SEM was performed using an FEI Quanta 200 3D system at room temperature (295 K). Secondary electron images using a 30 keV primary electron beam were captured in different regions of the specimen to observe the surface morphology after leaching.

A protective carbon coating of about 2 μm thickness was deposited in the region of interest prior to the FIB TEM lamellae preparation. The FIB lamellae were milled and polished using 30 keV Ga ions. In few cases, secondary electron images using 30 keV Ga ions were also captured to better observe the near-surface features. The TEM images and pores in the gels were analyzed using the Fiji software and its particle analysis tool.

For TEM analysis, the specimens were cooled to −130°C using a Gatan liquid nitrogen–cooled holder and a Hitachi 9500 microscope using 300 keV electrons (flux $<2 \times 10^{17}$ e^- cm^{-2} s^{-1}).

2.4.4 | Spectroscopic ellipsometry

Spectroscopic ellipsometry (SE) measurements were performed with a RC2 ellipsometer (J.A. Woollam Co.) with a light source that covers the wavelength range of 193–1000 nm. Measurements were conducted at an incident angles of 65°, 70°, and 75° to refractive indices of nonirradiated and irradiated CJ2 samples. Note that, in our experiment, ellipsometry could estimate the refractive index change associated with the irradiation but could not determine the thickness of the alteration layer due to severe degradation of the surface quality during the corrosion.

2.4.5 | Infrared spectroscopy

Infrared (IR) spectroscopy measurements were conducted in specular reflection geometry in a ~100 × 100 μm^2 surface area using a Bruker Hyperion 3000 FT-IR spectrometer equipped with a 15× reflective objective, which has incident and collection angles ranging from 11.3° to 26.3°. A gold surface was used as a reference, and spectra were obtained by averaging 400 scans with a resolution of 6 cm^{-1}.

2.4.6 | Sum frequency generation spectroscopy

The sum frequency generation (SFG) spectra were collected using an EKSPLA SFG spectrometer (EKSPLA, Lithuania). The measurements were performed in reflection geometry with a visible (532 nm) beam from the picosecond laser and a tunable IR beam from an optical parametric generator and amplifier (OPG/OPA), which was pumped by the picosecond laser at 1064 and 532 nm wavelengths. The IR and visible beams were overlapped spatially and temporally on the sample surface to generate the sum frequency photons. Produced sum frequency beam was then filtered using a monochromator and detected using a photomultiplier tube. The incident angles of the IR and visible beams were 56° and 60°, respectively. The spectra were collected as an average of 300 pulses in ssp polarization (s-polarized SFG, s-polarized visible, p-polarized IR) and in 10 cm^{-1} steps in the frequency range of 3000–4000 cm^{-1}. Collected sum-frequency spectra were normalized to IR and visible beam intensities to account for the laser power fluctuation.

2.5 | Computational methods

To better understand water mobility in pristine and irradiated glasses, classical molecular dynamics calculations have been performed. A hydrated glass with molar composition 62.1% SiO_2–14.3% Al_2O_3–13.5% Na_2O–10.1% H_2O (SANH) was prepared. This glass does not contain boron because no classical potentials are currently available to simulate hydrated borosilicate glasses. Only the SiO_2,

Al_2O_3, and Na_2O oxides mixed with H_2O have been considered.

The classical potentials used to prepare the systems have been completely described by Mahadevan et al.[14,29] These potentials use fixed and diffuse ionic charges to better represent the Coulombic interaction change versus interatomic distance.[38] Moreover, chemical water dissociation is allowed.

An 8 Å cutoff radius is applied for the potential terms in the real space. The Coulombic terms are calculated using the Wolf method[39] with an 8 Å radius. Each simulation box contains 5000 atoms. The time step is equal to .1 fs for all the preparation stages.

Different structures are prepared at ambient temperature by applying the following thermal scheme. A liquid is equilibrated at 4000 K during 2×10^6 time steps in the NVT ensemble starting from a random configuration. Then a thermal quench is applied from 4000 to 300 K. Three different quench rates, 5×10^{12}, 10^{15}, and 10^{16} K s^{-1}, were applied to stabilize structures at different depolymerization levels and densities. These quench rates will be called QR1, QR2, and QR3, respectively, thereafter. The thermal quenches are applied by decreasing the temperature per stages. At each intermediate temperature, a relaxation is performed in the NVT ensemble. The final system at 300 K is relaxed in the NPT ensemble during 2×10^5 time steps, then in the NVE ensemble during 50 000 time steps.

The three glasses prepared at the rates QR1, QR2, and QR3 are called, respectively, QR1_300K, QR2_300K, and QR3_300K.

The largest quench rates are used to mimic the radiation effects. In fact, it has been shown previously that accelerating the thermal quench allows to reproduce swelling, depolymerization, and an increase of the structural disorder[24,40–42] much faster than by accumulating displacement cascades.

Starting from the structures equilibrated at 300 K, structures at 550 K (respectively 800 K) have been prepared. We chose to work at 300, 550, and 800 K, that is, temperatures lower than the glass transition temperature, to investigate in particular the diffusion of the mobile elements (Na, H) in a rigid network to be closer to the experimental case. First, a relaxation in the NVT ensemble is performed at 550 K (respectively 800 K) during 10^6 time steps. Then a relaxation is performed in the NPT ensemble at 550 K (respectively 800 K) during 2×10^5 time steps to determine the new equilibrium volume. Finally, a relaxation is performed in the NVE ensemble at 550 K (respectively 800 K) during 50 000 time steps. The systems prepared at 550 K starting from the QR1_300K, QR2_300K, and QR3_300K systems will be called, respectively, QR1_550K, QR2_550K, and QR3_550K. In the same way, the systems prepared at 800 K will be called QR1_800K, QR2_800K, and QR3_800K.

Diffusion coefficients of the atomic species have been measured at 300, 550, and 800 K. For this, additional trajectories during 3×10^6 time steps were calculated in the NVT ensemble. The diffusion coefficients are estimated from the mean squared displacements:

$$D_i = \frac{1}{N_i} \lim_{t \to \infty} \frac{\sum_{n=1}^{N_i} \left| \vec{r}_i(t) - \vec{r}_i(t=0) \right|^2}{6t}$$

where D_i represents the diffusion coefficient of species i, N_i corresponds to the number of atoms of species i, and $r_i(t)$ and $r_i(t=0)$ correspond to the position of atom i at time t and initially.

3 | RESULTS

3.1 | Effect of irradiation on the glass structure evidenced by NMR and IR

^{29}Si, ^{11}B, ^{27}Al, and ^{23}Na NMR spectra were recorded on the pristine and irradiated CJ2 glass powders. A typical boron spectrum resolved into contributions from four (^4B) and three (^3B) coordinated species can be seen in Figure 1A. The high-intensity peak near −1 ppm represents ^4B units, and the broadband from ~2 to 17 ppm represents ^3B units, respectively.[36] After irradiation, the population of ^4B decreased. Further, the change in the shape of BO_3 peak suggests an increase in the B/Si mixing ratio after irradiation, which is confirmed by the isotropic projection of MQMAS experiments (Figure 1B), showing the mean resonance position of BO_3/BO_4 resonances according to their bonding (Angeli et al.,[36] Du et al.[43]). Note that BO_3(B/Si) are generally referred to as "ring" and "nonring" species; ring implies the formation of a supermolecular unit, thus a preferential bonding to boron. Using a common approach, four components were used to fit these spectra (two are needed at least for BO_3 and BO_4 resonances, respectively), as shown in Figure S2 and Table S1. The $\%BO_4$ decreased from 48 (±2)% to 37 (±2)%, notably with an increase of the BO_3(Si) units; thus, the reflectivity of the B/Si mixing increases.

In Figure 2A, ^{23}Na spectra of irradiated CJ2 show a decrease in the peak and a shift toward the left. The modifications are better seen in MQMAS experiments, as shown by the isotropic projection displayed in Figure 2B (2D MQMAS spectra are shown in Figure S3). These variations suggest both an increase of the average quadrupolar coupling constant (C_Q) and isotropic chemical shift (δ_{iso}). They are confirmed by the fit of the MAS NMR

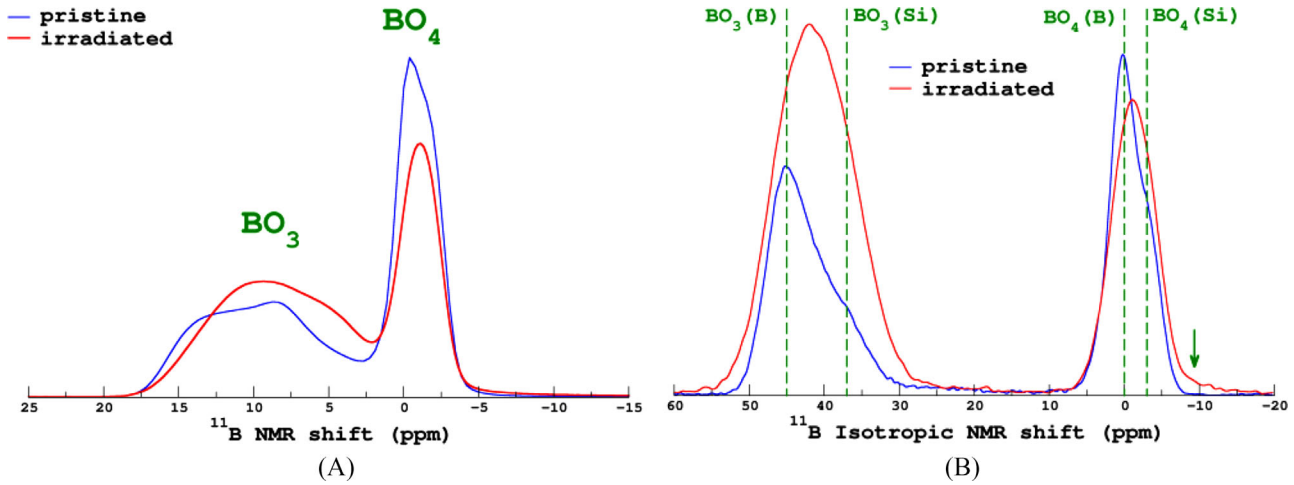

FIGURE 1 ^{11}B MAS and MQMAS NMR spectra of nonirradiated (pristine) and irradiated CJ2 powder. Part (A) shows the MAS NMR spectra and (B) the isotropic projection of the MQMAS spectra (see Figure S1).

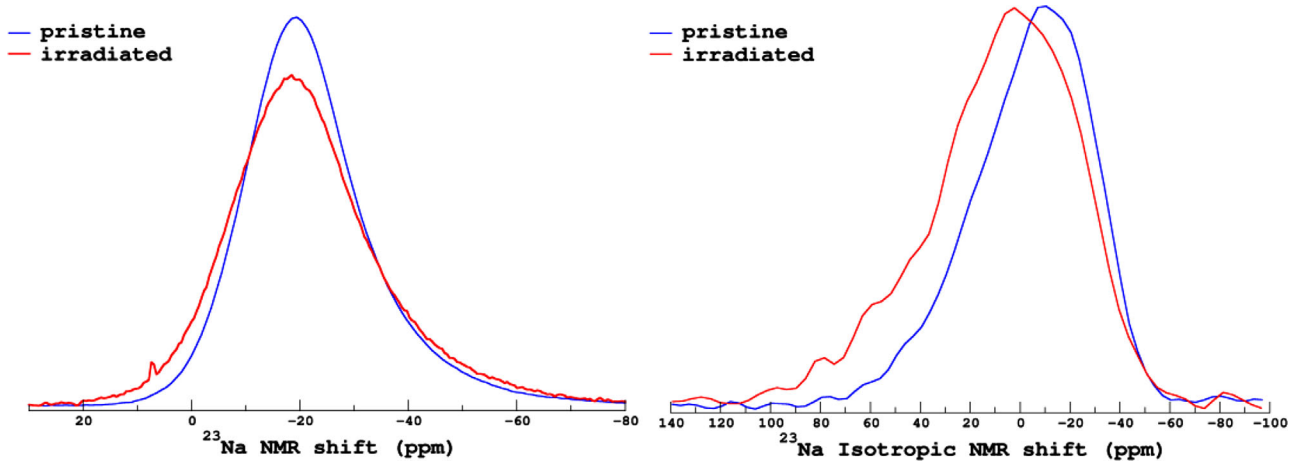

FIGURE 2 ^{23}Na MAS and MQMAS NMR spectra of nonirradiated (pristine) and irradiated CJ2 powders. Part (A) shows the MAS NMR spectra and (b) the isotropic projection of the MQMAS spectra (see Figure S3). The MAS NMR spectra are plotted normalized to the same area (not the isotropic projection of the MQMAS spectra that are normalized to the height maximum). Thus, the apparent reduction in the NMR spectra is mainly due to the broadening after irradiation.

spectra (see Figure S4 and Table S2). These variations suggest a decrease in the Na–O distance as discussed in Angeli et al.[44] The average distance between sodium and oxygen atoms is smaller when Na is associated with NBOs as compared to bridging oxygens. Thus, irradiated CJ2 is more depolymerized.

There is also a minor peak in the ^{23}Na MAS NMR of the irradiated sample between 0 and 10 ppm. This peak might be reflective of a slight surface alteration (hydrated and/or carbonated species), but it has not been investigated as it represents less than 1% of the sodium.

In Figure 3, the decrease in Q_4 entities and increase in Q_3 entities after irradiation are confirmed. In Figure 4, ^{27}Al spectra show a significant broadening and a change in the shape of the curve after irradiation, related to an increase of δ_{iso} and C_Q (see Figure S6 and Table S3), thus confirming the higher local disorder and chemical mixing. No AlO_5 were observed in MQMAS experiments (see Figure S5).

In conclusion, and as already observed in many previous works, NMR shows modification that are reflective of a significant modification of the network: increase of the B/Si mixing (^{11}B), decrease of the polymerization (^{23}Na, ^{29}Si), and AlO_4 units more distorted.

The decrease of the B coordination after irradiation by heavy ions is also detected by IR spectroscopy (Figure 5). It can be seen in Figure 5 that the amplitude of the band between 1300 and 1500 cm^{-1}, traditionally attributed to BO_3 local environments,[45–48] increases after irradiation. It

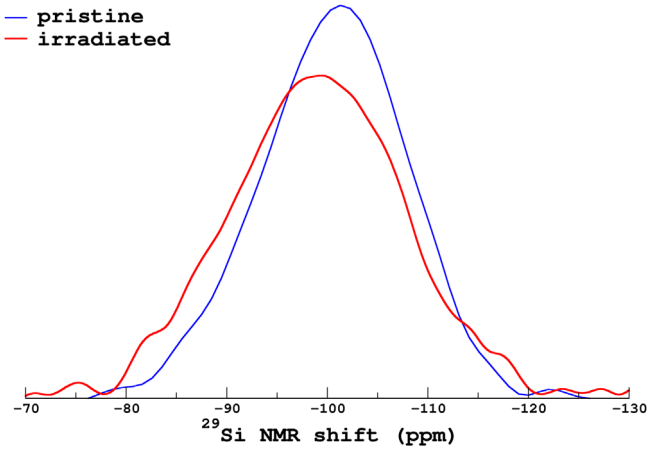

FIGURE 3 NMR spectra for irradiated and nonirradiated CJ2 powders of ^{29}Si. The MAS NMR spectra are plotted normalized to the same area. Thus, the apparent reduction in the NMR spectra is mainly due to the broadening after irradiation.

means that the BO_3 concentration increases due to BO_4 conversions into BO_3, consistent with the ^{11}B NMR result. The band between 900 and 1300 cm^{-1} is also modified. This band reflects the Si–O–Si connectivity. The reduction of Q_4 connectivity is responsible for the decrease of this band intensity[49,50] that is consistent with the ^{29}Si NMR result.

3.2 | Density modification

SE has been used to measure the refractive indexes in the pristine and irradiated CJ2 glass (Figure 6). The refractive index clearly decreases after irradiation and according to the Clausius–Mossotti relationship[51]; this modification can be explained by a density decrease. Swelling under heavy ion irradiation is a classical result already observed on other silicate glasses.

3.3 | Changes in hydrous species upon irradiation

To investigate how the depolymerization in the glass network and change in B coordination upon irradiation could modify nature of interfacial water, the SFG spectra of the nonirradiated and irradiated samples were measured at different relative humidity levels (Figure 7). The irradiated sample has a higher SFG intensity around 3750 cm^{-1}. This peak is associated with isolated silanol groups without hydrogen bonding interactions on the glass surface,[52] and the higher intensity implies a larger abundance of silanol groups in the irradiated glass surface.[52] The increase in the free silanol group density is likely due to the depolymerization. Furthermore, the overall intensity of the 3100–3500 cm^{-1} band is greater in the irradiated sample. This higher intensity indicates a higher abundance of structured water molecules on the irradiated surface.

3.4 | Initial dissolution rate experiment

Initial dissolution rate, r_0, of pristine and irradiated CJ2 glass monoliths was determined by monitoring the release of Si into the solution (Figure 8). It can be seen that the release is linear, and the trend intersects the *y*-axis very near zero, which are two criteria to verify that the rate is maximal. Furthermore, to confirm the reproducibility of the result, three tests were performed with irradiated glass. At 90°C and pH 9, r_0(pristine) and r_0(irradiated) were estimated to be ~2.46 and 14.22 ± 4.3 g m^{-2} d^{-1}, respectively. The r_0(pristine) is in agreement with the other experimental data reported in the literature, including a recent submitted paper by Gin et al.[37] The irradiated glass is estimated to dissolve ~5.6 times faster than the pristine one. Lönartz et al.[53] reported a three-time increase in the initial dissolution rate for a sodium borosilicate glass subjected to similar irradiation beams and corroded at 85°C and pH 7.

3.5 | Passivating gel formation

3.5.1 | Solution and ToF-SIMS analysis

To understand the irradiation impact on the gel layer formation, experiments were conducted with two irradiated and one pristine CJ2 monoliths in a Si-saturated solution, isotopically enriched in ^{29}Si and ^{18}O, at temperature 90°C and $pH^{90°C}$ of 9. The same initial solution was used for the three monoliths. The alteration parameters are given in Table 3.

Table 4 presents the analysis performed on the solution after the removal of altered monoliths on the 33rd day of the experiment. It can be noted that the Si final concentration in all three cases is close to the concentration of the starting solution ~339 mg L^{-1}. The ^{29}Si isotopic enrichment in the solution has dropped from an ^{29}Si/^{28}Si ratio of ~147 to ~70, which means that ~2 mg L^{-1} of ^{28}Si have been released from the glass. This corresponds to ~2–3 nm glass equivalent thickness dissolved into the solution.

A closer look at Table 4 clearly depicts the difference between pristine and irradiated CJ2 samples with respect to normalized boron loss and the corresponding equivalent altered thickness (*ET*(B)). *ET*(B) for the irradiated CJ2 (~4–5 μm) is almost two to three times higher than for the pristine CJ2 (~2 μm). The gel layer thickness for pristine CJ2 is in agreement with Gin et al.[37] The gel layer thickness

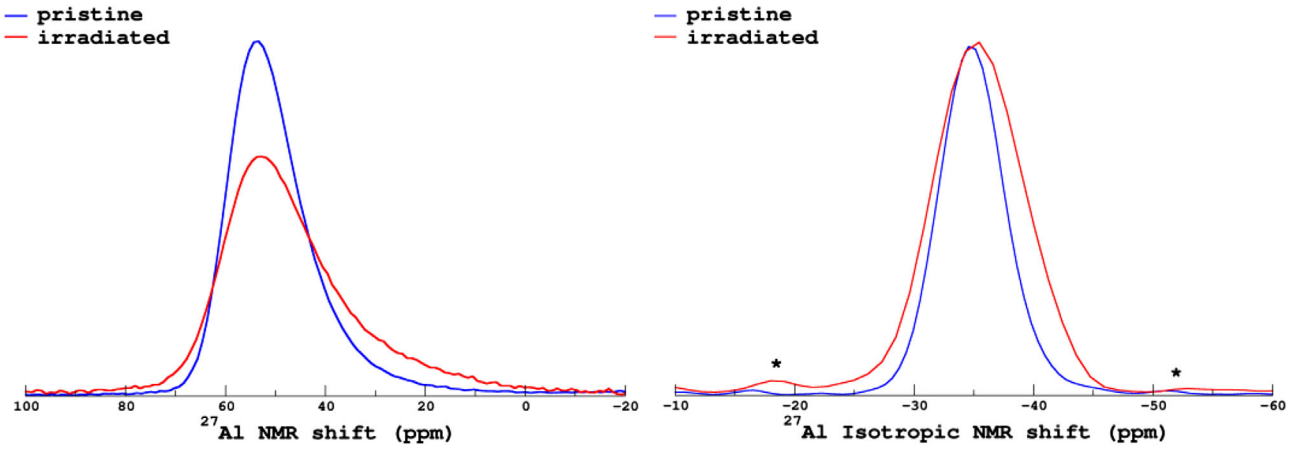

FIGURE 4 ^{27}Al MAS and MQMAS NMR spectra of nonirradiated (pristine) and irradiated CJ2 powders. Part (A) shows the MAS NMR spectra and (B) the isotropic projection of the MQMAS spectra (see Figure S5). The MAS NMR spectra are plotted normalized to the same area (not the isotropic projection of the MQMAS spectra that are normalized to the height maximum). Thus, the apparent reduction in the NMR spectra is mainly due to the broadening after irradiation.

TABLE 4 Analysis from solution data at the end of the 33-day long glass dissolution experiment on three glass coupons conducted in a silica-saturated and isotopically (^{29}Si and ^{18}O) spiked solution at 90°C and $pH^{90°C}$ of 9

Sample name	C_f(Si) (mg L^{-1})	NL(B) (g m^{-2})	ET(B) (μm)	^{29}Si/^{28}Si		Equivalent Si added from glass (μg)
CJ2_NIR	333.25	5.15	2.14	72.2	±2.0	.65
CJ2_IR_1	339.72	13.29	5.53	77.1	±2.4	.72
CJ2_IR_2	342.58	8.92	3.71	73	±2	1.00

Note: NIR and IR represent nonirradiated and IR irradiated coupons, respectively. C_f(Si) represents concentration of Si in the solution sample taken on the 33rd day. Normalized mass loss (NL) and equivalent thickness (ET) were calculated according to formulas given in Section 2.

estimated with solution analysis is close to the estimation from ToF-SIMS analysis (see Figures 9 and S7), 2.2 μm (CJ2_NIR), 6.6 μm (CJ2_IR_1), and 7.5 μm (CJ2_IR_2). For the sample CJ2_IR_2, it is suspected that there was perhaps an error while taking measurement for the dilution factor. The reason for the confidence in solution data estimation for CJ2_IR_1 is attributed to the generally observed agreement (within uncertainty) between solution data and the ToF-SIMS estimation of gel layer thickness, as seen here in the case CJ2 NIR sample too.[11]

Further, the ToF-SIMS analysis shows that the entire gel layer is uniformly enriched in ^{18}O, irrespective of whether it is derived from irradiated or pristine CJ2. The average estimation of ^{18}O isotopic enrichment in heart of the gel is .267 (CJ2_NIR), .22 (CJ2_IR_1), and .17 (CJ2_IR_2). Assuming the mass balance and that the solution (with $^{18}O/^{16}O$ = .453) was in equilibrium with the gel with respect to oxygen isotopic enrichment, it can be said that there is a decrease by 41% (CJ2_NIR), 51% (CJ2_IR_1), and 63% (CJ2_IR_2) in the $^{18}O/^{16}O$ isotopic ratio. The higher decrease noted for the irradiated samples could be explained by faster gel ripening limiting the O exchanges with the solution.

On the other hand for all three samples, a ^{29}Si enrichment was observed in the first tens of nanometers of the gel, and the rest of the gel layer was at the natural abundance (Figure 10). It means that no exchange occurs within the gel volume between the Si from the glass and from the solution.

Solution analysis and ToF-SIMS profiles are in good agreement with the recent experiments conducted under similar conditions by Gin et al.[37] for CJ2 glass composition. Even though the initial rate of glass dissolution, as seen in previous section, was five times faster for the irradiated CJ2 and the layer thickness was two to four times higher for irradiated CJ2, the global mechanism followed for the gel layer formation was the same, that is, partial hydrolysis and in situ reorganization.

In addition, to investigate the reactivity of the gels developed on altered CJ2_NIR and CJ2_IR_1 with respect to water, monoliths removed from the leaching solution were rinsed with few drops of 97.1% ^{18}O water and kept covered

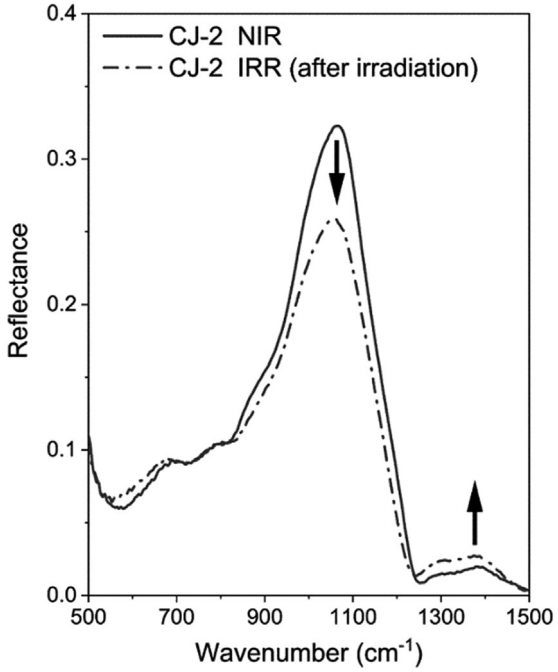

FIGURE 5 Infrared (IR) spectra for irradiated and nonirradiated CJ2 monoliths. The modifications after irradiation are underlined by arrows.

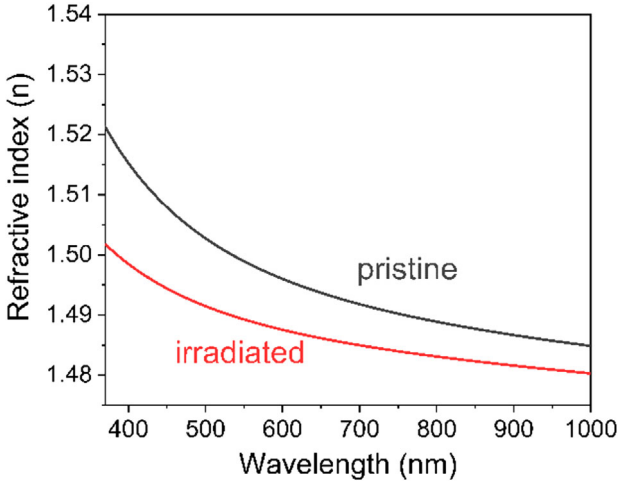

FIGURE 6 Spectroscopic ellipsometry in the pristine and irradiated CJ2 glasses

for couple of hours at room temperature with this solution until ToF-SIMS analysis was performed under cryogenic mode. It can be observed (Figure S7) that for CJ2_IR_1, an outer layer of ~100 nm thickness possessing ^{18}O enrichment is slightly higher than the starting leaching solution, whereas for CJ2_NIR, no significant signature of isotopic exchange with 97.1% ^{18}O solution is seen. This indicates the higher diffusivity of the external layer of the gel formed on irradiated CJ2.

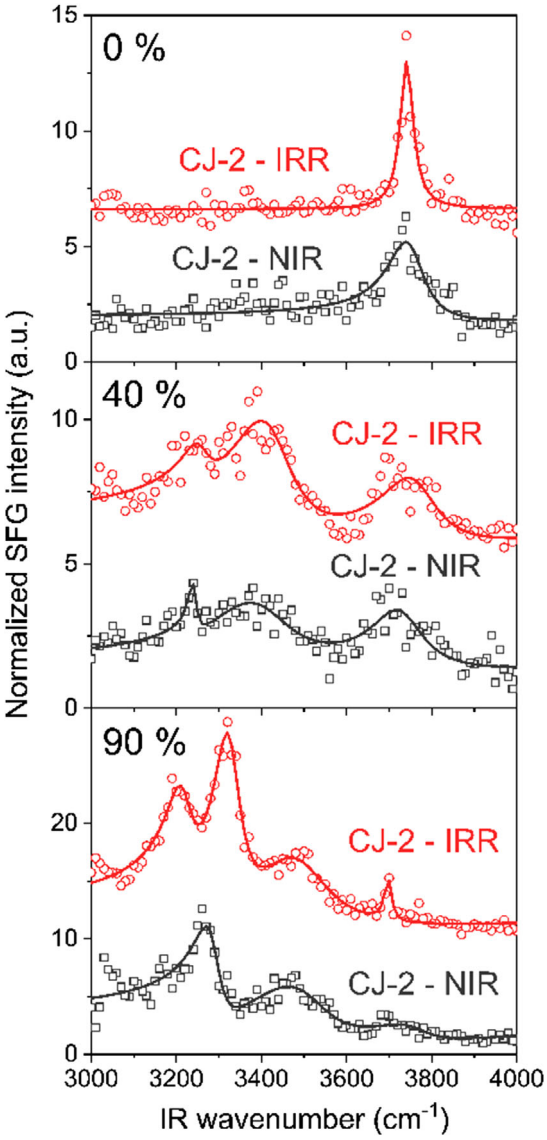

FIGURE 7 Sum frequency generation (SFG) spectra measured in the pristine and preirradiated CJ2 coupons under different relative humidity (RH) levels

3.5.2 | TEM analysis

To analyze the morphology of the alteration layer in the CJ2_NIR and CJ2_IR_1 coupons after removal from leaching solution and ToF-SIMS analysis, SEM and TEM observations have been performed. The SEM observations are described in Figures S8–S10. We will concentrate here only on the TEM observations.

In Figure 11, TEM analysis estimates the depth of gel layer for CJ2_NIR to be around 1.9–2 μm, which is in excellent agreement with the solution and ToF-SIMS data. The images show that the gel layer is nonporous or perhaps the pore size is below the TEM resolution (in this case <.5 nm). On the other hand, in Figure 12, CJ2_IR_1 is seen to

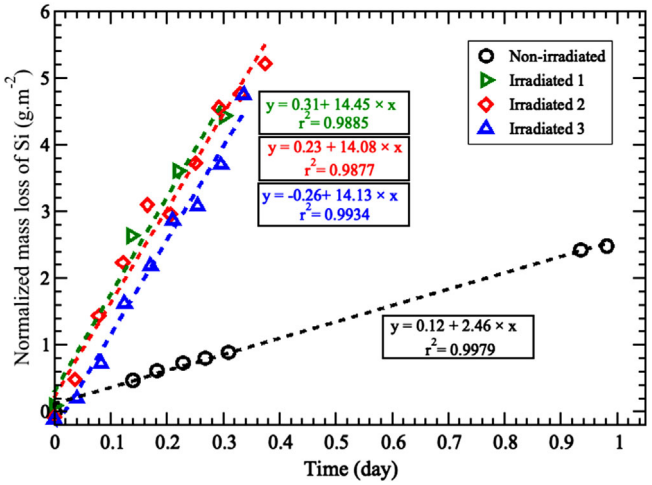

FIGURE 8 Si-normalized mass loss with time for irradiated and nonirradiated CJ2 glasses in dilute conditions at 90°C and pH 9. Red, green, and blue markers correspond to the three sets of data for irradiated CJ2 glass coupon. Black markers correspond to dataset for nonirradiated CJ2.

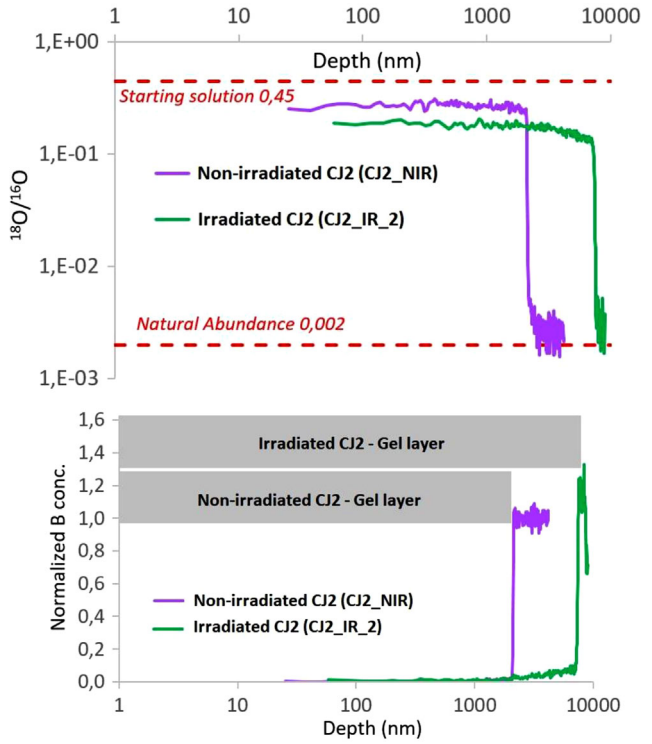

FIGURE 9 Time-of-flight secondary-ion-mass-spectrometry (ToF-SIMS) characterization of altered CJ2 glass coupons (the nonirradiated and the CJ2_IR_2 sample) resulting from the short-term test conducted at 90°C and $pH^{90°C}$ of 9. $^{18}O/^{16}O$ (top) and normalized B-profiles (bottom). The gel/glass interface is located at 2.2 and 7.4 μm below the outer surface for the nonirradiated and the irradiated CJ2_IR_2 samples, respectively.

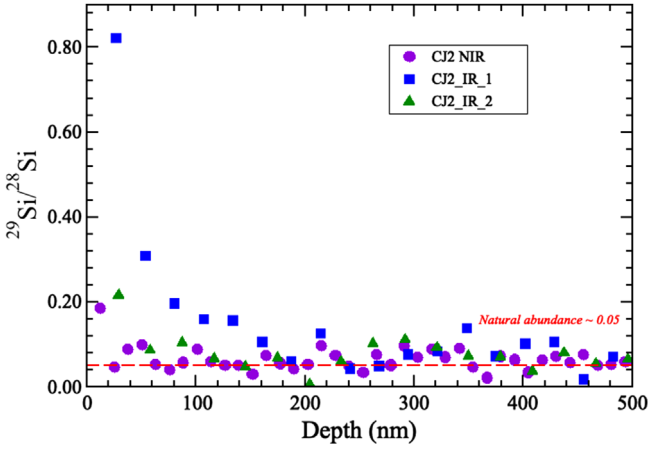

FIGURE 10 Time-of-flight secondary-ion-mass-spectrometry (ToF-SIMS) characterization of altered CJ2 glass coupons (one nonirradiated and two irradiated) resulting from the short-term test conducted at 90°C and $pH^{90°C}$ of 9. $^{29}Si/^{28}Si$ in the starting solution was 147 ± 9. After the removal of the glass monoliths on the 33rd day, the leached solution had $^{29}Si/^{28}Si$ ratio as ~72, ~77, and ~73 for one nonirradiated and two irradiated altered samples, respectively.

TABLE 5 Densities (g cm^{-3}) of the simulated SANH glass versus the thermal quench rate

Quench rate	QR1	QR2	QR3
Density	2699	2531	2444

possess a nano-porous gel layer with typical pore size less than 4 nm. Tribet et al.[54] also observed a porous gel layer for irradiated–altered ISG sample and nonporous layer for the nonirradiated-altered ISG sample under similar alteration conditions.

3.6 | Molecular dynamics simulations

3.6.1 | Impact of the thermal quench rate on the glass structures

In this section, the structural characteristics of the simulated SANH glass prepared at different quench rates are compared. By accelerating the thermal quench, density decreases (Table 5). The swelling is equal to 6.6% between the QR1 and QR2 quench rates.

In Table 6, the Si and Al coordination numbers versus the thermal quench rate are given. The Si atoms remain in a tetrahedral coordination whatever the quench rate. A decrease of the Al average coordination number is observed when the thermal quench rate increases.

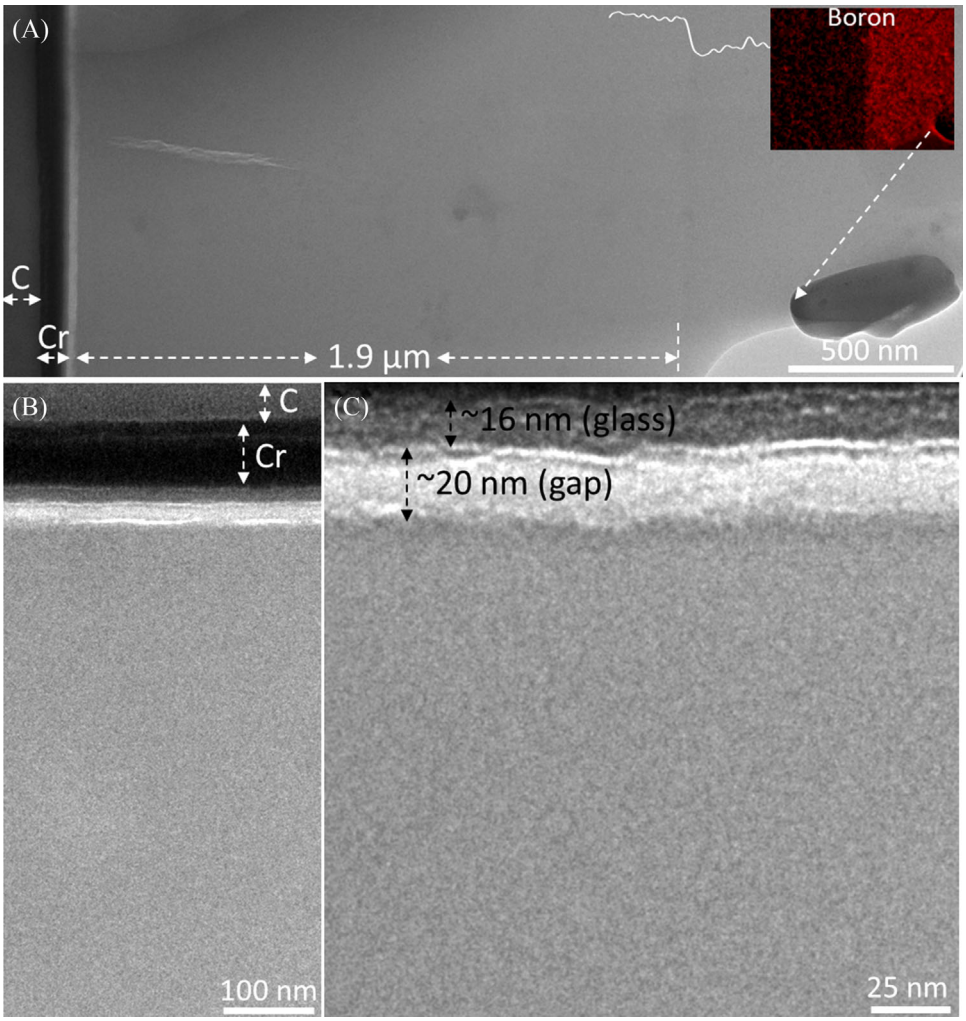

FIGURE 11 BF-TEM images of pristine CJ2_NIR glass leached for 33 days at 90°C and $pH^{90°C}$ of 9: (A) a low-magnification TEM image showing protective carbon and Cr layers deposited prior to FIB lamella preparation. This is followed by the altered glass with an alteration layer of about 1.9 μm (demarcated by the vertical dashed line from the nonaltered glass). A transmitted electron intensity profile across the alteration boundary is shown in white color. A boron EF-TEM map near the interface shows boron depletion in the altered layer; (B) a medium magnification image to better visualize the gap separating the thin glass layer from the rest of the alteration layer; and (C) higher magnification image to better visualize the gap

TABLE 6 Si and Al coordination numbers versus the thermal quench rate

	QR1	QR2	QR3
Si average coordination number	4,0	4,0	4,0
Si4 (%)	100	100	100
Al average coordination number	4,16	4,04	4,05
Al3 (%)	.23	1.56	1.06
Al4 (%)	84.25	92.80	93.34
Al5 (%)	14.96	5.45	5.51
Al6 (%)	.56	.19	.08

TABLE 7 Nonbridging, two, and tri coordinated O percentages versus the thermal quench rate

	QR1 (%)	QR2 (%)	QR3 (%)
O_1	12.08	15.74	15.80
O_2	82.87	77.43	77.17
O_3	5.05	6.83	7.03

In Table 7, the percentages of nonbridging, two, and tri coordinated oxygen atoms are indicated versus the quench rate. It can be noted that the percentages of nonbridging and tri coordinated O atoms increase with the thermal quench rate.

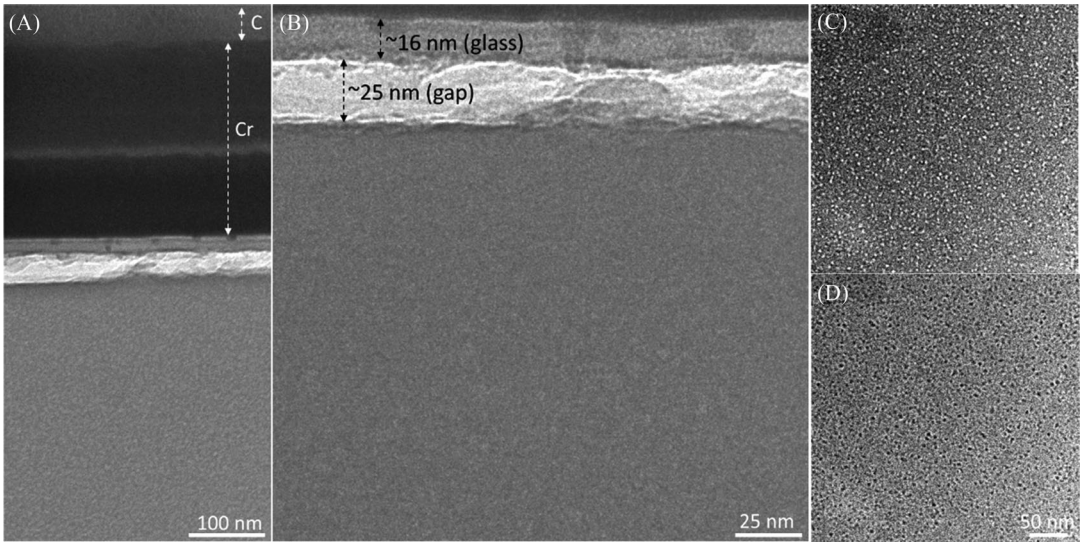

FIGURE 12 BF-TEM images of irradiated CJ2_IR_1 glass leached for 33 days at 90°C and $pH^{90°C}$ of 9: (A) A low-magnification TEM image showing protective carbon and Cr layers deposited prior to FIB lamella preparation (the Cr layer was deposited twice explaining the bright region in the middle of the Cr layer possibly as a result of oxidation of the first deposited layer). This is followed by the altered glass that was found to contain a uniform distribution of pores; (B) a higher magnification image to better visualize the gap separating the thin glass layer on top of the specimen from rest of the alteration layer; and (C and D) high magnification under and overfocus images showing typical pores in the alteration layer (image defocus = 4000 nm)

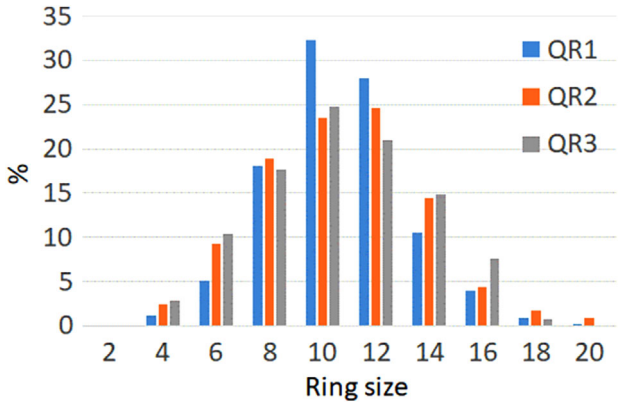

FIGURE 13 King ring size distributions (in percentages) for the different thermal quench rates

The King ring[55] size distributions (in percentages) are compared on Figure 13. The ring size corresponds here to the quantity of oxygen and formers forming the rings. It can be noted that the quantity of small (size lower than 6) and large (size larger than 14) rings increases when the quench rate increases. On the contrary, the quantity of intermediate rings (size between 8 and 12) decreases when the thermal quench rate increases. It means that the topological disorder increases with the thermal quench rate. This result is in good agreement with previous simulations.[21,56–58]

The topological disorder increase can also be observed on the bond angle distributions. On Figure 14, the Si–O–Si and Si–O–Al bond angle distributions are plotted. The distributions widen when the quench rate increases, whereas the average Si–O–Si and Si–O–Al angles decrease. The Si–O–Si angle decreases from 151.5° to 146.6° between the QR1 and QR2 thermal quench rates, and the Si–O–Al average angle decreases from 139.0° to 134.4°. These decreases are correlated to the glass depolymerization, as observed previously in other silicate glass compositions.[59,60]

Globally, by increasing the thermal quench rate, the depolymerization level increases, and the density and the topological order decrease. In parallel, the King ring size and bond angle distributions widen. All these processes were also observed when a glassy structure is subject to a series of displacement cascades. Hence, increasing the thermal quench rate allows to reproduce qualitatively the ballistic effects.

3.6.2 | Impact of the thermal quench rate on the diffusion coefficients

The diffusion coefficients estimated in the simulated systems prepared at 300, 550, and 800 K are detailed here. The diffusion coefficients for the five species are compared on Figure 15. Only the results obtained with the QR1 (5×10^{12} K s^{-1}) and QR2 (10^{15} K s^{-1}) thermal quench rates are shown. The results obtained with the QR3 thermal quench rate (10^{16} K s^{-1}) are not usable, and we will explain why later.

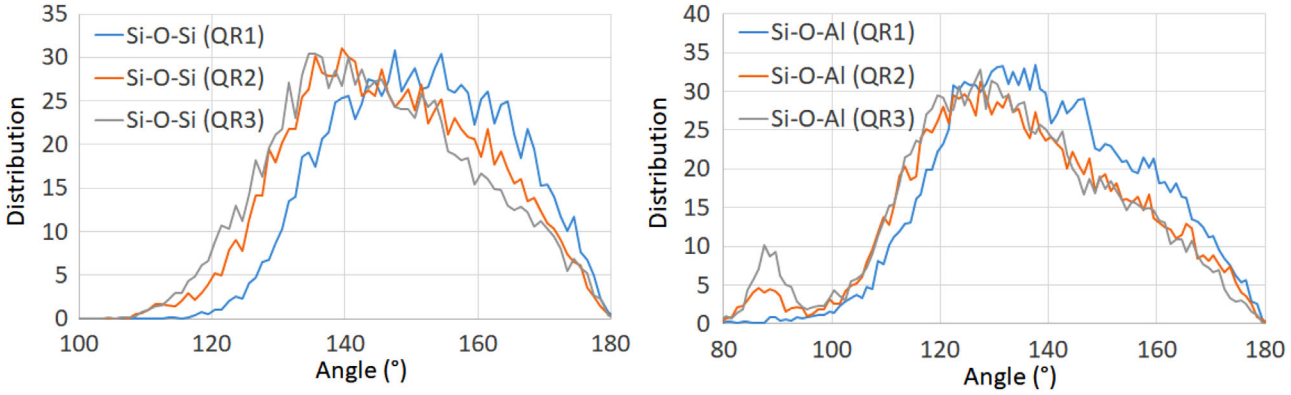

FIGURE 14 Si–O–Si and Si–O–Al bond angle distributions for the different thermal quench rates

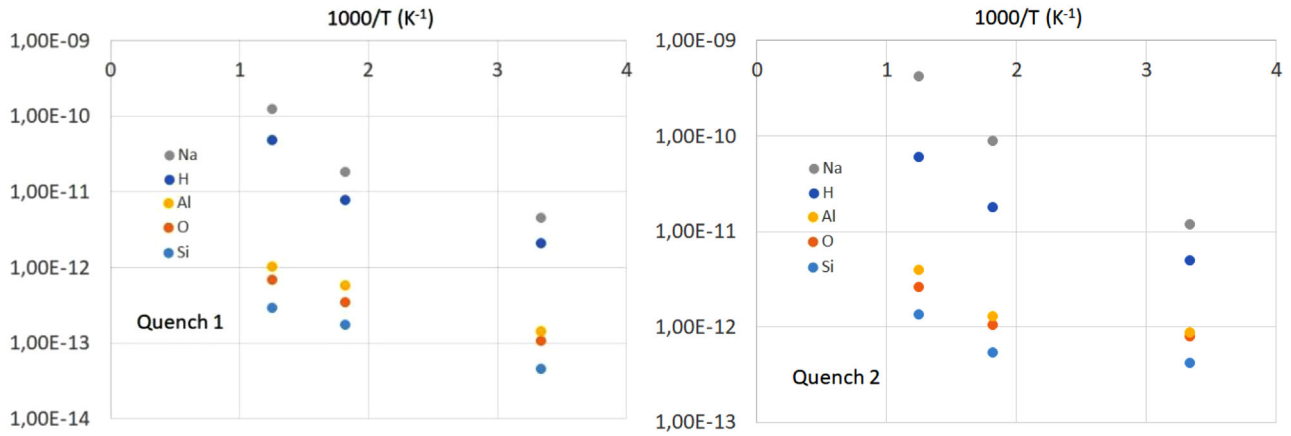

FIGURE 15 Diffusion coefficients (in $m^2\ s^{-1}$) for the five different species in the systems prepared at the thermal quench rates QR1 (left) and QR2 (right)

The hierarchy of the diffusion coefficients are the same: $D_{Na} > D_H > D_{Al} > D_O > D_{Si}$ for QR1 and QR2. The hierarchy between Si, Al, and O corresponds to what has been observed previously for dry gels prepared with the same potentials[61] and also to Stein et al. results in dry silicate glasses.[62] Na mobility is larger than H mobility probably because of stronger H–O interactions than Na–O interactions. Larger alkali than hydrogen mobilities have already been observed experimentally in different silicate glasses.[63]

When the quench rate increases, the diffusion coefficients shift toward larger values. The depolymerization and swelling induced by accelerating the thermal quench rate allow easier atomic motions. This result is not in contradiction with the diffusion decrease observed after glass annealing,[64] with the hardness decrease observed after modifying the glass thermal history,[65] or with the electrical conductivity increase observed after swelling.[66] A correlation between alkaline diffusion coefficient and network connectivity has also been recently evidenced in simulated SiO_2–Al_2O_3–Na_2O glasses by Zhao et al.[67] The temperature used in this latter work is greater than the ones used here, and quantitative comparisons are difficult.

The diffusion coefficients measured in the system quenched at QR3 are shown on Figure 16. Nonphysical results are obtained. In particular, the Si, Al, and O diffusion coefficients decrease between 550 and 800 K, which is surprising. It is probably because the QR3 thermal quench rate is too high, and the system is not correctly stabilized at 300 K. In consequence, additional relaxations occur during the annealing at 550 and 800 K explaining nonlinear effects on the diffusion coefficients. Nevertheless, the hierarchy $D_{Na} > D_H > D_{Al} > D_O > D_{Si}$ remains valid.

In Figure 17, the two groups, (Si, Al, O) and (Na, H), are separated. The significant accelerations of the diffusion between QR1 and QR2 are clearly visible.

The diffusion coefficient ratios between QR2 and QR1 are plotted on Figure 18. The ratios are larger than 6 for (Si, Al, O) and larger than 2 for (Na, H). Hence, swelling and depolymerization have a significant impact

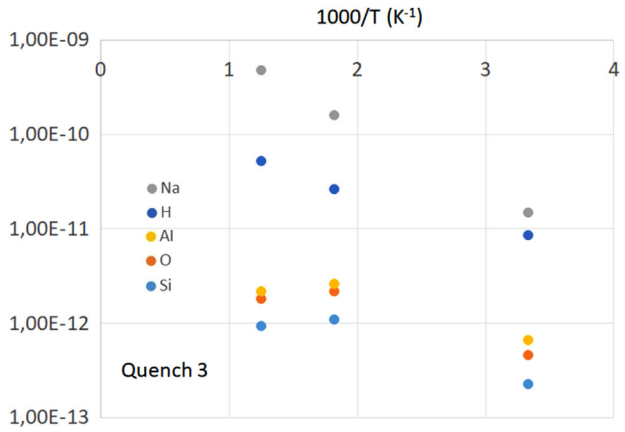

FIGURE 16 Diffusion coefficients (in $m^2\ s^{-1}$) for the five different species in the systems prepared at QR3

on the diffusion, and this impact is larger for formers than modifiers.

4 | DISCUSSION

Confinement of the radionuclides in borosilicate glass matrices on the geological timescales is subject to the durability of borosilicate glass under aqueous corrosion. Recent work by Mougnaud et al.,[68] Tribet et al.,[54] and Lönartz et al.,[53] including this work, have reported a significant effect of a preirradiation by heavy ions on the initial glass dissolution rate and gel thickness in residual rate regime. However, why heavy ion irradiation leads into the increase in the glass corrosion rate is not clearly understood.

Two corrosion regimes, stage I and the beginning of stage II, have been investigated here. Stage I corresponds to the initial glass network hydrolysis, whereas stage II corresponds to the B and Na releases by exchange with aqueous species conjointly to the passivating gel layer formation.

It has been concluded previously,[69] considering complex glasses, that the radiation effect was insignificant on the initial alteration rate. Two factors may explain this observation. First, the complexity of the glass studied, with more than 30 components, was much larger. In addition, it has been shown that radiation effects in complex glasses are reduced,[32,70] but the decrease is not huge. Second, the irradiation sources were different. Doped glasses or glasses irradiated by lower energy beams were considered. Both the glass complexity and a different irradiation scheme could possibly have mitigated the damage.

In this work, in order to decouple the effect of irradiation and glass composition, a simplified glass containing four oxides was preirradiated with heavy ions before performing the alteration experiments.

4.1 | Radiation impact on the forward rate regime

At the beginning, glass could be attacked either by simple diffusion (H_2O) or ion-exchange and interdiffusion between the protonated species (H^+, H_3O^+) in the solution and the alkalis in the glass. Simultaneously, nucleophilic attack by OH^- on the ionic–covalent bonds of network-forming elements (Si–O–X, where X = Si, Al, B) results into network hydrolysis. The Si atoms released in solution during this corrosion stage comes from glass hydrolysis. As long as the solution is sufficiently diluted, the glass continues to dissolve at the initial rate.

Here we show that a preirradiation by heavy ions induces a significant increase, by a factor of 5.6, of the initial alteration rate. This effect can be correlated to the structural modifications induced by irradiation. Based on NMR, IR, SE, SFG, and classical molecular dynamics simulations, it has been observed that irradiation leads to boron coordination and density decrease, and NBO concentration and topological disorder increase. These changes in the glass network could have implications on the interaction of glass with water molecules.

These changes can explain an increase of the initial dissolution rate. In fact, it has been shown that three coordinated B atoms are more soluble than four coordinated B atoms.[71,72] Moreover, molecular simulations have demonstrated that the hydrolysis energy for one Si atom decreases when the depolymerization level in its local environment increases.[73,74] The calculations presented here show that the diffusion coefficients are systematically larger in depolymerized and less dense structures. Finally, we can consider that swelling, by opening larger free volumes, could increase the glass–solution contact surface and favor the dissolution rate. Hence, several structural modifications induced by irradiation could affect the initial alteration rate. Similar orders of magnitude for the alteration rate increase after irradiation have been recently reported for the ISG glass, and similar explanations could be brought to explain these results.[68]

It is quite surprising that insignificant increase of the initial alteration rate in more complex glasses was previously reported.[69,75] As said previously, irradiation by heavy ions leads to lower density, and hardness changes in complex glasses compared to simple glasses, but the changes are not so large. For example, under irradiation by heavy ions (Au), the swelling in the complex SON68 glass is equal to 2%, whereas it is equal to 2.7% in the 6-oxides ISG glass.[70] This question remains unclear.

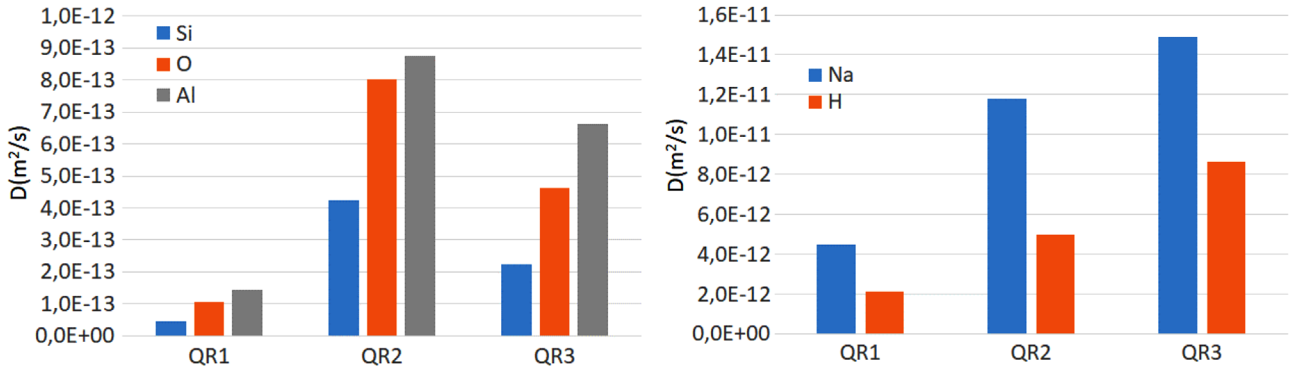

FIGURE 17 Comparison of the diffusion coefficients versus the thermal quench rate

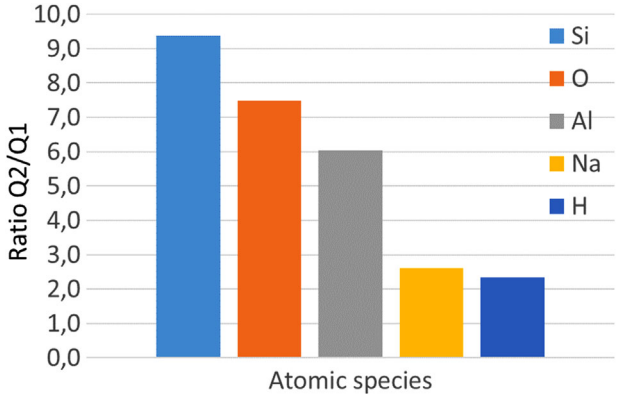

FIGURE 18 Diffusion coefficient ratios between the QR2 and QR1 thermal quench rates

4.2 | Radiation effect on passivating gel formation

To study the alteration layer formation mechanisms, CJ2 glass monoliths were altered in a Si-saturated medium traced with ^{29}Si and ^{18}O. Irradiated glass was reported to have two to three times deeper gel layer than the pristine one. Globally, the mechanisms followed for the gel layer formation remained qualitatively the same, with partial hydrolysis and in situ reorganization. This conclusion is driven based on the observation that the alteration layers for the pristine and preirradiated glasses are both enriched in ^{18}O, whereas they are not enriched in ^{29}Si. If the Si atoms belonging to the glass were first dissolved before precipitation, the gel layer would be enriched in ^{29}Si. The CJ2 glass–reticulated network is only partly hydrolyzed.

Yet several differences remained between the alteration layers formed on the pristine and irradiated glasses. First, the alteration layer thickness is significantly larger on the preirradiated glass. As the initial dissolution rate is larger after irradiation, this result is quite normal if we consider isovolumetric glass dissolution (the volume of gel is same as the volume of altered glass).

Further, TEM results estimated the alteration layer formed on the irradiated monolith to be more porous in contrast to non- or low-porous alteration layer formed on the pristine sample (or at least with pore sizes below the TEM resolution).

This result is very interesting, and two points can be underlined. It is possible that the alteration layer topology keeps the memory of the initial glass structure leading quickly to the formation of a more open structure if the initial glass is less dense and more depolymerized. This conclusion is also supported by another study using tracing solutions and by a previous study in which radiation traces formed before alteration by ^{252}Cf remained visible in the alteration gel.[76]

Moreover, it has been shown in a previous paper that the residual alteration rate for the preirradiated glass is significantly larger than for the pristine one. In addition, this alteration rate decreases with time. It is possible that the ripening of the alteration layer formed on the preirradiated glass accelerates, leading to larger pores because of a faster coalescence of the small ones.

A global process could be proposed to explain the significant increase of the gel layer thickness after preirradiation. As water diffusion largely increases in a preirradiated glass as demonstrated by classical molecular dynamics simulations, the depth of the hydrated layer (the part of the glass experiencing water diffusion before B and Na releases) will increase (or at least the interface between this hydrated layer and the pristine glass will progress faster). It can be considered that the gel layer is formed after the transformation of this hydrated layer into gel due to B and Na releases in solution and structural relaxation. If the hydrated layer structure retains the memory of the initial glass structure, it will be less dense and polymerized. Hence, a possible acceleration of the hydrated layer–gel layer transformation after a preirradiation by heavy ions because of a decrease of the hydrated layer rigidity.

5 | CONCLUSIONS

A SiO_2–Al_2O_3–B_2O_3–Na_2O glass with the same molar ratios as in the French SON68 nuclear glass and ISG has been investigated. Pristine and preirradiated (952 MeV, ^{136}Xe) monoliths were altered in DIW to measure the initial alteration rate, and in a solution enriched with ^{29}Si and ^{18}O to measure the residual alteration rate.

Qualitatively, the alteration behavior is not modified after preirradiation. In the pristine and preirradiated glasses, the gel is enriched with ^{18}O but not with ^{29}Si, which means that the dissolution occurs through in situ hydrolysis and local reorganization instead of complete hydrolysis followed by precipitation.

After preirradiation, the initial alteration rate increases by a factor of 5.6, and the depth of the alteration layer increases by a factor between 2 and 3. The glass density decreases after irradiation, and in parallel, its depolymerization level and topological disorder increase. By using classical molecular dynamics, it has been shown that these modifications induce water diffusion acceleration possibly at the origin of the initial alteration rate increase.

In addition, SEM and TEM observations showed that the alteration layer structure is modified after preirradiation. It can be suspected that the alteration layer keeps the memory of the initial glass structure, and that the gel ripening is faster for the preirradiated glass. The gel ripening corresponds to the coalescence of smaller pores into larger ones.

For the future, it will be necessary to better characterize the correlation between the initial glass structure and the alteration layer topology using both experiments and molecular simulations.

ACKNOWLEDGMENTS

This work was supported as part of the Center for Performance and Design of Nuclear Waste Forms and Containers, an Energy Frontier Research Center funded by the U.S. Department of Energy, Office of Science, Basic Energy Sciences under Award Number: DE-SC0016584. A. H. Mir is thankful to the Engineering and Physical Sciences Research Council for funding under Early career Fellowship grant EP/ T012811/1.

ORCID

Jean-Marc Delaye https://orcid.org/0000-0002-1311-642X
Seong H. Kim https://orcid.org/0000-0002-8575-7269
Thibault Charpentier https://orcid.org/0000-0002-3034-1389
Stephane Gin https://orcid.org/0000-0002-1950-9195

REFERENCES

1. Gin S, Jollivet P, Tribet M, Peuget S, Schuller S. Radionuclides containment in nuclear glasses: an overview. Radiochim Acta. 2017;105(11, SI):927–59. https://doi.org/10.1515/ract-2016-2658
2. Ojovan MI, Lee WE. Glassy wasteforms for nuclear waste immobilization. Metall Mater Trans A—Phys Metall Mater Sci. 2011;42A(4):837–51. https://doi.org/10.1007/s11661-010-0525-7
3. Ojovan MI, Lee WE. An introduction to nuclear waste immobilization. Amsterdam: Elsevier Science Publisher BV; 2005.
4. Gin S, Delaye J-M, Angeli F, Schuller S. Aqueous alteration of silicate glass: state of knowledge and perspectives. NPJ Mater Degrad. 2021;5(1):42. https://doi.org/10.1038/s41529-021-00190-5
5. Conradt R. Chemical durability of oxide glasses in aqueous solutions: a review. J Am Ceram Soc. 2008;91(3):728–35. https://doi.org/10.1111/j.1551-2916.2007.02101.x
6. Vienna JD, Ryan J V, Gin S, Inagaki Y. Current understanding and remaining challenges in modeling long-term degradation of borosilicate nuclear waste glasses. Int J Appl Glas Sci. 2013;4(4, SI):283–94. https://doi.org/10.1111/ijag.12050
7. Geisler T, Nagel T, Kilburn MR, Janßen AC, Icenhower JP, Fonseca ROC, et al. The mechanism of borosilicate glass corrosion revisited. Geochim Cosmochim Acta. 2015;158:112–29. https://doi.org/10.1016/j.gca.2015.02.039
8. Hellmann R, Cotte S, Cadel E, Malladi S, Karlsson LS, Lozano-Perez S, et al. Nanometre-scale evidence for interfacial dissolution-reprecipitation control of silicate glass corrosion. Nat Mater. 2015;14(3):307–11. https://doi.org/10.1038/nmat4172
9. Ruiz-Agudo E, Putnis CV, Putnis A. Coupled dissolution and precipitation at mineral-fluid interfaces. Chem Geol. 2014;383:132–46. https://doi.org/10.1016/j.chemgeo.2014.06.007
10. Gin S, Collin M, Jollivet P, Fournier M, Minet Y, Dupuy L, et al. Dynamics of self-reorganization explains passivation of silicate glasses. Nat Commun. 2018;9(1):2169. https://doi.org/10.1038/s41467-018-04511-2
11. Gin S, Jollivet P, Fournier M, Angeli F, Frugier P, Charpentier T. Origin and consequences of silicate glass passivation by surface layers. Nat Commun. 2015;6:6360. https://doi.org/10.1038/ncomms7360
12. Mir AH, Jan A, Delaye J-M, Donnelly S, Hinks J, Gin S. Effect of decades of corrosion on the microstructure of altered glasses and their radiation stability. NPJ Mater Degrad. 2020;4(1). https://doi.org/10.1038/s41529-020-0115-0
13. Gin S, Mir AH, Jan A, Delaye JM, Chauvet E, De Puydt Y, et al. A general mechanism for gel layer formation on borosilicate glass under aqueous corrosion. J Phys Chem C. 2020;124(9):5132–44. https://doi.org/10.1021/acs.jpcc.9b10491
14. Damodaran K, Delaye J-M, Kalinichev AG, Gin S. Deciphering the non-linear impact of Al on chemical durability of silicate glass. Acta Mater. 2022;225:117478. https://doi.org/10.1016/j.actamat.2021.117478
15. Vienna JD, Crum VJ. Non-linear effects of alumina concentration on Product Consistency Test response of waste glasses. J Nucl Mater. 2018;511:396–405. https://doi.org/10.1016/j.jnucmat.2018.09.040
16. Gin S, Abdelouas A, Criscenti LJ, Ebert WL, Ferrand K, Geisler T, et al. An international initiative on long-term behavior of high-level nuclear waste glass. Mater Today. 2013;16(6):243–8. https://doi.org/10.1016/j.mattod.2013.06.008

17. Advocat T, Crovisier JL, Vernaz E, Ehret G, Charpentier H. Hydrolysis of R7T7 nuclear waste glass in dilute media – mechanisms and rate as a function of ph. In: Abrajano TA, Johnson LH, editors. Symposium P – scientific basis for nuclear waste management XIV. 1991;212:57–64. https://doi.org/10.1557/PROC-212-57
18. Gin S, Beaudoux X, Angeli F, Jegou C, Godon N. Effect of composition on the short-term and long-term dissolution rates of ten borosilicate glasses of increasing complexity from 3 to 30 oxides. J Non-Cryst Solids. 2012;358(18–19):2559–70. https://doi.org/10.1016/j.jnoncrysol.2012.05.024
19. Mir AH. Radiation effects on oxide glasses: importance of energy deposition and relaxation processes. PhD thesis. 2015.
20. Peuget S, Delaye J-M, Jegou C. Specific outcomes of the research on the radiation stability of the French nuclear glass towards alpha decay accumulation. J Nucl Mater. 2014;444(1–3):76–91. https://doi.org/10.1016/j.jnucmat.2013.09.039
21. Jan A, Delaye J-M, Gin S, Kerisit S. Molecular dynamics simulation of ballistic effects in simplified nuclear waste glasses. J Non-Cryst Solids. 2019;505:188–201. https://doi.org/10.1016/j.jnoncrysol.2018.11.021
22. Maugeri EA, Peuget S, Staicu D, Zappia A, Jegou C, Wiss T. Calorimetric study of glass structure modification induced by a decay. J Am Ceram Soc. 2012;95(9, SI):2869–75. https://doi.org/10.1111/j.1551-2916.2012.05304.x
23. Weber WJ, Ewing RC, Angell CA, Arnold GW, Cormack AN, Delaye JM, et al. Radiation effects in glasses used for immobilization of high-level waste and plutonium disposition. J Mater Res. 1997;12(8):1946–78. https://doi.org/10.1557/jmr.1997.0266
24. Kieu L-H, Kilymis D, Delaye J-M, Peuget S. Discussion on the structural origins of the fracture toughness and hardness changes in rapidly quenched borosilicate glasses: a molecular dynamics study. Procedia Mater Sci. 2014;7(Complete):262–71. https://doi.org/10.1016/j.mspro.2014.10.034
25. Perez A, Daval D, Fournier M, Vital M, Delaye J-M, Gin S. Comparing the reactivity of glasses with their crystalline equivalents: the case study of plagioclase feldspar. Geochim Cosmochim Acta. 2019;254:122–41. https://doi.org/10.1016/j.gca.2019.03.030
26. Bunker BC. Molecular mechanisms for corrosion of silica and silicate-glasses. J Non-Cryst Solids. 1994;179:300–8. https://doi.org/10.1016/0022-3093(94)90708-0
27. Gin S, Guo X, Delaye J-M, Angeli F, Damodaran K, Testud V, et al. Insights into the mechanisms controlling the residual corrosion rate of borosilicate glasses. NPJ Mater Degrad. 2020;4(1):41. https://doi.org/10.1038/s41529-020-00145-2
28. Gin S, Frugier P, Jollivet P, Bruguier F, Curti E. New insight into the residual rate of borosilicate glasses: effect of S/V and glass composition. Int J Appl Glas Sci. 2013;4(4, SI):371–82. https://doi.org/10.1111/ijag.12048
29. Mahadevan TS, Sun W, Du J. Development of water reactive potentials for sodium silicate glasses. J Phys Chem B. 2019;123(20):4452–61. https://doi.org/10.1021/acs.jpcb.9b02216
30. Mahadevan TS, Garofalini SH. Dissociative chemisorption of water onto silica surfaces and formation of hydronium ions (vol 112, 1514,2008). J Phys Chem C. 2008;112(14):5694. https://doi.org/10.1021/jp8015134
31. Ziegler JF, Ziegler MD, Biersack JP. SRIM - The stopping and range of ions in matter (2010). Nucl Instrum Methods Phys Res Sect B—Beam Interact Mater Atoms. 2010;268(11–12):1818–23. https://doi.org/10.1016/j.nimb.2010.02.091
32. Mir AH, Monnet I, Toulemonde M, Bouffard S, Jegou C, Peuget S. Mono and sequential ion irradiation induced damage formation and damage recovery in oxide glasses: stopping power dependence of the mechanical properties. J Nucl Mater. 2016;469:244–50. https://doi.org/10.1016/j.jnucmat.2015.12.004
33. Mir AH, Peuget S. Using external ion irradiations for simulating self-irradiation damage in nuclear waste glasses: state of the art, recommendations and, prospects. J Nucl Mater. 2020;539:152246. https://doi.org/10.1016/j.jnucmat.2020.152246
34. Neeway J, Abdelouas A, Grambow B, Schumacher S. Dissolution mechanism of the SON68 reference nuclear waste glass: new data in dynamic system in silica saturation conditions. J Nucl Mater. 2011;415(1):31–7. https://doi.org/10.1016/j.jnucmat.2011.05.027
35. Bouakkaz R, Abdelouas A, El Mendili Y, Grambow B, Gin S. SON68 glass alteration under Si-rich solutions at low temperature (35-90 degrees C): kinetics, secondary phases and isotopic exchange studies. RSC Adv. 2016;6(76):72616–33. https://doi.org/10.1039/c6ra12404f
36. Angeli F, Charpentier T, de Ligny D, Cailleteauz C. boron speciation in soda-lime borosilicate glasses containing zirconium. J Am Ceram Soc. 2010;93(9):2693–704. https://doi.org/10.1111/j.1551-2916.2010.03771.x
37. Gin S, Jegou C, Sessegolo L, Bisbrouck N, Jan A, Tribet M, Delaye J.-M., Angeli F.. Effects of irradiation on the mechanisms controlling the residual rate of an alumino-borosilicate glass. NPJ Mater Degrad. 2022;6(1):59. https://doi.org/10.1038/s41529-022-00266-w
38. Guillot B, Guissani Y. How to build a better pair potential for water. J Chem Phys. 2001;114(15):6720–33. https://doi.org/10.1063/1.1356002
39. Wolf D, Keblinski P, Phillpot SR, Eggebrecht J. Exact method for the simulation of Coulombic systems by spherically truncated, pairwise r(-1) summation. J Chem Phys. 1999;110(17):8254–82. https://doi.org/10.1063/1.478738
40. Delaye J-M, Peuget S, Calas G, Galoisy L. Comparative effects of thermal quenching and ballistic collisions in SiO_2-B_2O_3-Na_2O glass. Nucl Instrum Methods Phys Res Sect B—Beam Interact Mater Atoms. 2014;326:256–9. https://doi.org/10.1016/j.nimb.2013.10.061
41. Kieu L-H, Delaye J-M, Stolz C. Modeling the effect of composition and thermal quenching on the fracture behavior of borosilicate glass. J Non-Cryst Solids. 2012;358(23):3268–79. https://doi.org/10.1016/j.jnoncrysol.2012.07.037
42. Kilymis DA, Delaye JM. Nanoindentation of pristine and disordered silica: molecular dynamics simulations. J Non-Cryst Solids. 2013;382:87–94. https://doi.org/10.1016/j.jnoncrysol.2013.10.013
43. Du LS, Stebbins JF. Solid-state NMR study of metastable immiscibility in alkali borosilicate glasses. J Non-Cryst Solids. 2003;315(3):239–55. https://doi.org/10.1016/S0022-3093(02)01604-6
44. Angeli F, Villain O, Schuller S, Ispas S, Charpentier T. Insight into sodium silicate glass structural organization by multinuclear NMR combined with first-principles calculations. Geochim Cosmochim Acta. 2011;75(9):2453–69. https://doi.org/10.1016/j.gca.2011.02.003

45. Kamitsos EI. Infrared studies of borate glasses. Phys Chem Glas. 2003;44(2):79–87.
46. Lepicard A, Cardinal T, Fargin E, Adamietz F, Rodriguez V, Richardson K, et al. Surface reactivity control of a borosilicate glass using thermal poling. J Phys Chem C. 2015;119(40):22999–3007. https://doi.org/10.1021/acs.jpcc.5b07139
47. Gautam CR, Yadav AK, Singh AK. A review on infrared spectroscopy of borate glasses with effects of different additives. ISRN Ceram. 2012;2012(5):428497. https://doi.org/10.5402/2012/428497
48. El-Egili K. Infrared studies of Na_2O-B_2O_3-SiO_2 and Al_2O_3-Na_2O-B_2O_3-SiO_2 glasses. Physica B—Condens Matter. 2003;325(1–4):340–8. https://doi.org/10.1016/S0921-4526(02)01547-8
49. Liu H, Kaya H, Lin Y-T, Ogrinc A, Kim SH. Vibrational spectroscopy analysis of silica and silicate glass networks. J Am Ceram Soc. 2022;105(4):2355–84. https://doi.org/10.1111/jace.18206
50. Liu H, Hahn SH, Ren M, Thiruvillamalai M, Gross TM, Du J, et al. Searching for correlations between vibrational spectral features and structural parameters of silicate glass network. J Am Ceram Soc. 2020;103(6):3575–89. https://doi.org/10.1111/jace.17036
51. Varshneya AK. Fundamentals of inorganic glasses. 3rd ed. Amsterdam: Elsevier; 1994. https://doi.org/10.1016/C2009-0-21359-6
52. Ngo D, Hongshen L, Chen Z, Kaya H, Zimudzi TJ, Gin S, et al. Hydrogen bonding interactions of H_2O and SiOH on a boroaluminosilicate glass corroded in aqueous solution. NPJ Mater Degrad. 2020;4(1):1. https://doi.org/10.1038/s41529-019-0105-2
53. Lönartz MI, Dohmen L, Lenting C, Trautmann C, Lang M, Geisler T. The effect of heavy ion irradiation on the forward dissolution rate of borosilicate glasses studied in situ and real time by fluid-cell Raman spectroscopy. Materials (Basel). 2019;12(9):1480. https://doi.org/10.3390/ma12091480
54. Tribet M, Mir AH, Gillet C, Jegou C, Mougnaud S, Hinks JA, et al. New insights about the importance of the alteration layer/glass interface. J Phys Chem C. 2020;124(18):10032–44. https://doi.org/10.1021/acs.jpcc.0c02121
55. Le Roux S, Jund P. Ring statistics analysis of topological networks: new approach and application to amorphous GeS_2 and SiO_2 systems. Comput Mater Sci. 2010;49(1):70–83. https://doi.org/10.1016/j.commatsci.2010.04.023
56. Delaye J-M, Peuget S, Bureau G, Calas G. Molecular dynamics simulation of radiation damage in glasses. J Non-Cryst Solids. 2011;357(14, SI):2763–8. https://doi.org/10.1016/j.jnoncrysol.2011.02.026
57. Delaye J-M, Le Gac A, Macaluso S, Angeli F, Lodesani F, Charpentier T, et al. Investigation of alumino-silicate glasses by coupling experiments and simulations: Part II—Radiation effects. J Non-Cryst Solids. 2021;569:120969. https://doi.org/10.1016/j.jnoncrysol.2021.120969
58. Kilymis DA, Delaye JM, Ispas S. Density effects on the structure of irradiated sodium borosilicate glass: a molecular dynamics study. J Non-Cryst Solids. 2016;432(B):354–60. https://doi.org/10.1016/j.jnoncrysol.2015.10.031
59. Angeli F, Delaye JM, Charpentier T, Petit JC, Ghaleb D, Faucon P. Investigation of A1-O-Si bond angle in glass by Al-27 3Q-MAS NMR and molecular dynamics. Chem Phys Lett. 2000;320(5–6):681–7. https://doi.org/10.1016/S0009-2614(00)00277-3
60. Lee SK, Stebbins JF. Disorder and the extent of polymerization in calcium silicate and aluminosilicate glasses: O-17NMR results and quantum chemical molecular orbital calculations. Geochim Cosmochim Acta. 2006;70(16):4275–86. https://doi.org/10.1016/j.gca.2006.06.1550
61. Taron M, Delaye J-M, Gin S. A classical molecular dynamics simulation method for the formation of ‘‘dry{’’} gels from boro-aluminosilicate glass structures. J Non-Cryst Solids. 2021;553:120513. https://doi.org/10.1016/j.jnoncrysol.2020.120513
62. Stein DJ, Spera FJ. Molecular dynamics simulations of liquids and glasses in the system $NaAlSiO_4$-SiO_2: physical properties and transport mechanisms. Am Mineral. 1996;81(3–4):284–302.
63. Doremus RH. Interdiffusion of hydrogen and alkali ions in a glass surface. J Non-Cryst Solids. 1975;19(Dec):137–44. https://doi.org/10.1016/0022-3093(75)90079-4
64. Shelby JE. Effect of thermal history on helium diffusion and solubility in vitreous B_2O_3 and sodium borate glasses. J Appl Phys. 1973;44(10):4588–91. https://doi.org/10.1063/1.1662005
65. Smedskjaer MM, Jensen M, Yue Y. Effect of thermal history and chemical composition on hardness of silicate glasses. J Non-Cryst Solids. 2010;356(18–19):893–7. https://doi.org/10.1016/j.jnoncrysol.2009.12.030
66. Angel PW, Hann RE, Cooper AR. Thermal history effects on electrical relaxation and conductivity for potassium silicate glass with low alkali concentrations. J Non-Cryst Solids. 1995;183(3):277–89. https://doi.org/10.1016/0022-3093(94)00588-5
67. Zhao Y, Du J, Qiao X, Cao X, Zhang C, Xu G, et al. Ionic self-diffusion of Na_2O-Al_2O_3-SiO_2 glasses from molecular dynamics simulations. J Non-Cryst Solids. 2020;527:119734. https://doi.org/10.1016/j.jnoncrysol.2019.119734
68. Mougnaud S, Tribet M, Renault J-P, Gin S, Peuget S, Podor R, et al. Heavy ion radiation ageing impact on long-term glass alteration behavior. J Nucl Mater. 2018;510:168–77. https://doi.org/10.1016/j.jnucmat.2018.07.046
69. Tribet M, Rolland S, Peuget S, Broudic V, Magnin M, Wiss T, et al. Irradiation impact on the leaching behavior of HLW glasses. In: Angeli F, Delaye JM, Schuller S, Pinet O, Rebiscoul D, Gin S, Peuget S, editors. 2ND Int. SUMMER Sch. Nucl. Glas. WASTEFORM Struct. Prop. LONG-TERM Behav. (SUMGLASS 2013). vol. 7. 2014. p. 209–15. https://doi.org/10.1016/j.mspro.2014.10.027
70. Karakurt G, Abdelouas A, Guin J-P, Nivard M, Sauvage T, Paris M, et al. Understanding of the mechanical and structural changes induced by alpha particles and heavy ions in the French simulated nuclear waste glass. J Nucl Mater. 2016;475:243–54. https://doi.org/10.1016/j.jnucmat.2016.04.022
71. Bunker BC, Arnold GW, Day DE, Bray PJ. The effect of molecular-structure on borosilicate glass leaching. J Non-Cryst Solids. 1986;87(1–2):226–53. https://doi.org/10.1016/S0022-3093(86)80080-1
72. Stone-Weiss N, Bradtmueller H, Eckert H, Goel A. Composition-structure-solubility relationships in borosilicate glasses: toward a rational design of bioactive glasses with controlled dissolution behavior. ACS Appl Mater Interfaces. 2021;13(27):31495–513. https://doi.org/10.1021/acsami.1c07519

73. Pelmenschikov A, Strandh H, Pettersson LGM, Leszczynski J. Lattice resistance to hydrolysis of Si-O-Si bonds of silicate minerals: ab initio calculations of a single water attack onto the (001) and (111) beta-cristobalite surfaces. J Phys Chem B. 2000;104(24):5779–83. https://doi.org/10.1021/jp994097r
74. Kagan M, Lockwood GK, Garofalini SH. Reactive simulations of the activation barrier to dissolution of amorphous silica in water. Phys Chem Chem Phys. 2014;16(20):9294–301. https://doi.org/10.1039/c4cp00030g
75. Wellman DM, Icenhower JP, Weber WJ. Elemental dissolution study of Pu-bearing borosilicate glasses. J Nucl Mater. 2005;340(2–3):149–62. https://doi.org/10.1016/j.jnucmat.2004.10.166
76. Dran JC, Petit JC, Brousse C. Mechanism of aqueous dissolution of silicate-glasses yielded by fission tracks. Nature. 1986;319(6053):485–7. https://doi.org/10.1038/319485a0

SUPPORTING INFORMATION

Additional supporting information can be found online in the Supporting Information section at the end of this article.

How to cite this article: Jan A, Delaye J-M, Kaya H, Kim SH, Mir AH, Charpentier T, et al. Radiation effects on the structure and alteration behavior of an SiO_2–Al_2O_3–B_2O_3–Na_2O glass. Int J Appl Glass Sci. 2023;14:113–132. https://doi.org/10.1111/ijag.16618